Asian Journal of Chemistry; Vol. 33, No. 12 (2021), 2999-3005

ASIAN JOURNAL OF CHEMISTRY

https://doi.org/10.14233/ajchem.2021.23418

A Facile Synthesis for Studying the Effect of Molar Concentration on Structural, Morphological and Optical Behaviour of MoO_3 Thin Films using Jet Nebulizer Spray Pyrolysis Technique for n-MoO_3/p-Si Photodiode Application

G. LAVANYA and N. SIVANANDAN*

Department of Electronics, PSG College of Arts and Science, Coimbatore-641014, India

*Corresponding author: E-mail: sivanandannanjan@gmail.com

Received: 17 July 2021; *Accepted*: 2 September 2021; *Published online*: 6 December 2021; AJC-20592

In this study, molybdenum trioxide (MoO_3) thin films were coated with various Mo concentrations 1, 2, 3 and 4 wt.% referred as L1, L2, L3 and L4 respectively on to the silica substrate calcined at 450 ºC by a facile, rapid cost-effective and a custom-made jet nebulizer spray pyrolysis (JNSP) technique. The concentration impact on the structural, morphological and compositional parameters were examined by XRD, FESEM, EDX, FTIR and Raman studies. The XRD peaks confirmed the presence of the orthorhombic phase of MoO_3 (α-MoO_3) in the prepared films. FESEM images depicted their nanorod structured morphology. EDX spectra confirm the presence of elements such as oxygen (O) and molybdenum (Mo). Molecular fingerprint of the samples were diagnosed by probing their molecular vibrations through the Raman Spectroscopy. Vibrational frequencies of the bonds in the samples was investigated by FTIR. The I-V measurements were analyzed in light and dark conditions for the n-MoO_3/p-Si junction diode.

Keywords: Molybdenum trioxide, Structural, Orthorhombic phase, Raman.

INTRODUCTION

In recent years, oxide semiconductor thin films have become an interesting topic in the field of material research particularly transition metal-oxides which play a vital role in many technological applications [1,2]. Metal oxide-based nanomaterials with notable electrical, mechanical and optical properties kindled the interest in many researches and finds a potential place in nano devices. Among them, molybdenum trioxide (MoO_3) has gained major attention because of its unique layered structure. It became a noteworthy progressive material with high electrical conductivity and optical transmittance in the visible region and also it possesses relative chemical stability and high refractive index. MoO_3 is a wide band gap (2.39-3.0 eV) transition metal oxide semiconductor with three different crystal structures [3,4]. They are orthorhombic phase (α-MoO_3), which is thermodynamically stable and the others are metastable namely monoclinic phase (β-MoO_3) and hexagonal phase (h-MoO_3) [5]. These 3 phases differ in their physical and chemical properties. MoO_3 has a probable application in solar cells, gas sensors, diodes, batteries, pseudocapacitors, biomedical researches [6], waveguides [7] and solid catalyst [8].

Properties of MoO_3 thin films depend very strongly upon the deposition techniques and their parameters. MoO_3 thin films can be synthesized using various physical and chemical deposition techniques such as physical vapour deposition, chemical vapour deposition, electron deposition, SILAR, sputtering, sol-gel, spray pyrolysis, thermal oxidation, nebulizer spray pyrolysis [9,10], *etc*. Despite various methods, spray pyrolysis is the most suitable and economically reliable method [11]. The other methods demand less time, energy and money at a larger scale, which makes them difficult to be scaled up.

Particularly jet nebulizer spray pyrolysis (JNSP) is a new non-vacuum method which allows large scale deposition of high-quality films in single-step heating at a low cost. Additionally, this technique offers a great advantage, namely, the material can be deposited at a relatively low temperature with low precursor material and also with various nanostructures. The low cost portable pocket-sized nebulizer affords reliable MoO_3 film coatings on a wide range of desired host surfaces. It is

feasible in producing a pinhole-free, uniform coating through controlling aerosol droplet distribution [12,13]. The preparative parameters such as the concentration of the starting solution, substrate temperature, deposition rate and time were optimized for better coatings.

Beside this, limited information is available on the structural, optical and electrical properties of MoO_3 thin films. In this work, the fabrication of pure MoO_3 thin films with variable Mo concentrations (1, 2, 3 and 4 wt.%) namely L1, L2, L3 and L4 on to the silica substrate is demonstrated by an innovative, facile rapid and cost-effective, custom-made JNSP technique. Later the synthesized films were subjected to the various characterization techniques, such as X-ray diffraction (XRD), field emission scanning electron microscopy (FESEM), energy dispersive X-ray (EDX), atomic force microscopy (AFM), ultraviolet-visible-near infrared (UV-Vis-NIR) spectroscopy, Fourier transform infrared (FTIR) and Raman spectroscopy. In order to determine the effect of various molybdenum concentrations on the structural, morphological, optical properties of pure MoO_3 thin films.

EXPERIMENTAL

Film deposition: To prepare pure MoO_3 thin films, ammonium molybdate tetrahydrate [$(NH_4)_6Mo_7O_{24}\cdot 4H_2O$] was used as a precursor material and dissolved in 20 mL of double-distilled water and stirred about 1 h in the magnetic stirrer to make 0.1 M starting solution. This aqueous ammonium molybdate tetrahydrate was used as a coating solution and the films were deposited on the silica substrate calcined at 450 ºC. The aerosols generated from the nebulizer undergoes successive pyrolysis due to the temperature gradient between the substrate (450 ºC) and the nozzle gun and finally, MoO_3 is decomposed on the substrate. The reaction describing the formation of MoO_3 from the precursor solution (aqueous ammonium molybdate tetrahydrate) is given below:

$$(NH_4)_6Mo_7O_{24}\cdot 4H_2O \longrightarrow 7MoO_3(s) + 6NH_3(g) + 7H_2O(g)$$

Here, Mo concentration was changed from 1, 2, 3 and 4 in wt%. Fig. 1 shows the scheme of jet nebulizer spray pyrolysis (JNSP) technique unit.

RESULTS AND DISCUSSION

X-ray diffraction (XRD): The structural analysis of the fabricated samples was carried out by XRD and the obtained XRD peak profiles are depicted in Fig. 2. The diffraction peaks of all 4 samples have higher intensities at planes (*hkl*) values of (110), (120) and (021). The slight variations in their corresponding 2θ values indicates the anisotropic growth of nanorods in the deposited films. The intensities of these major peaks vary with various concentrations. These prominent peaks confirmed the presence of orthorhombic phase of MoO_3 (α-MoO_3) in the prepared samples with respect to JCPDS file no. 89-5108.

The average crystallite size of the synthesized samples at the preferred orientation was calculated by using Scherrer's formula:

$$D = \frac{k\lambda}{\beta\cos\theta} \quad (1)$$

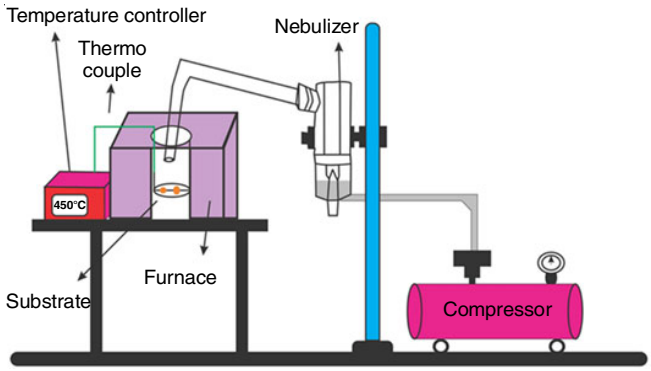

Fig. 1. Scheme of jet nebulizer spray pyrolysis (JNSP) technique unit

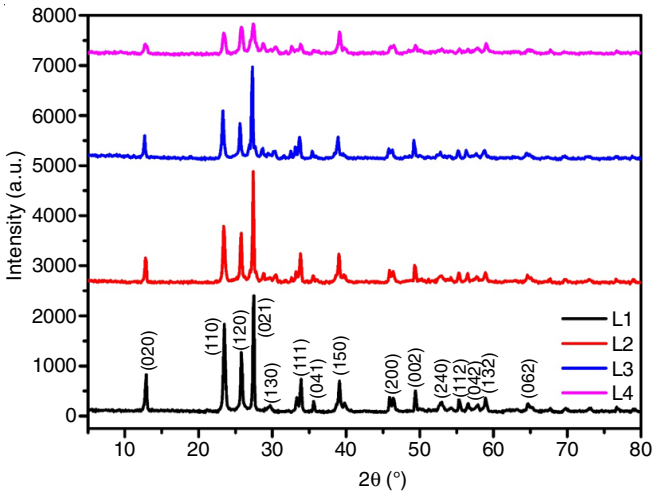

Fig. 2. XRD patterns of the L1, L2, L3 and L4 thin films

where, D = average crystallite size, k = constant (depends on the shape of the crystallite, miller indices and Bragg determined its value as 0.9), λ = wavelength of the incident radiation, β = broadening of the diffraction line (FWHM) and θ = Bragg's diffraction angle.

Crystallite size and lattice strain are two main parameters which affects the peak widths, intensities and the shift of 2θ peak positions [14]. Here, the crystallite size obtained by Scherrer's formula (~ 14-32 nm) and the calculated micro-strain (eqn. 3) were plotted against different MoO_3 mole-fractions (Fig. 3).

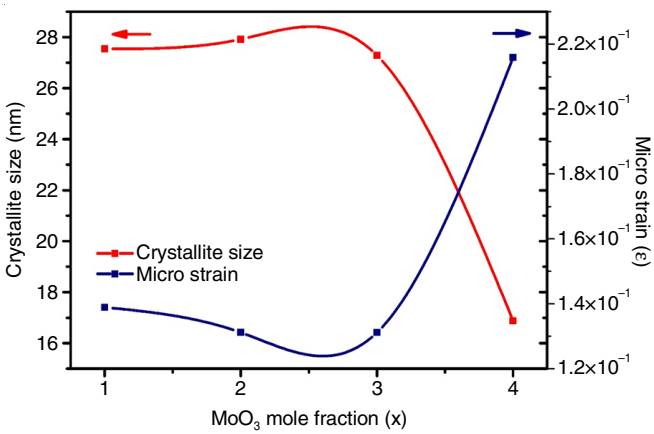

Fig. 3. Average crystallite size and micro-strain for different mole fractions of MoO_3

Dislocation densities (δ) and microstrains (ε) were calculated using the below relations:

$$\delta = \frac{1}{D^2} \quad (2)$$

$$\varepsilon = \frac{\lambda}{D\sin\theta} - \frac{\beta}{\tan\theta} \quad (3)$$

The determined interplanar spacing (d_{hkl}), grain size, FWHM, dislocation density (δ), micro strain (ε) and lattice constants (a b c) values are listed in Table-1.

Variations in the lattice constants for various concentrations is due to the development of some strains upon increasing the concentrations. Dislocation density decreases with an increment in the grain size shown in Fig. 4. Interplanar spacing increases with the increase in concentration, since the bigger size of ions brings the expansion in the lattice which may generate the deformations in the lattice. Microstrains obtained from the eqn. 3 ranges from ~ 0.11 to 0.24 lin^{-2} m^{-4}, respectively.

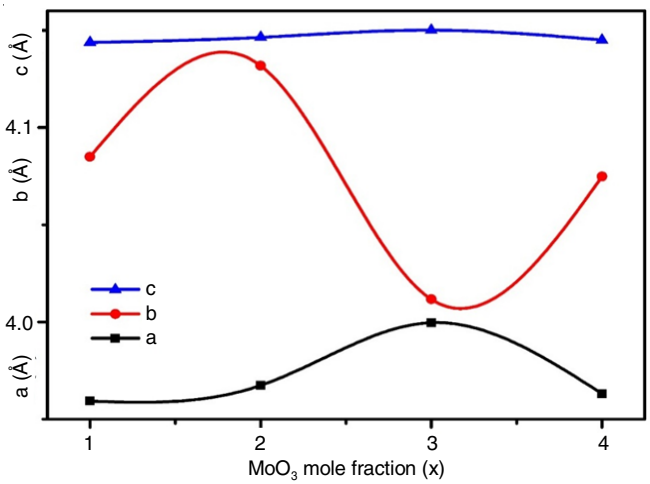

Fig. 4. Variations in lattice constants a, b and c with the mole fraction

FESEM studies: The surface morphology of the prepared samples is studied using FESEM. The FESEM images of MoO_3 at various concentrations taken at 2 μm are shown in Fig. 5. Rod-like nanostructures are clearly observed. The size of the micro-rods (~ 4-0.8 μm) decreases gradually as the concentration of MoO_3 increases. This can be inferred from the length of the microrods observed. The microrods are uniformly distributed without any holes or cracks having a smooth surface. The images depict a clearly disturbed surface with randomly oriented islets-like structures [15]. The aggregation of the micro-rods is due to physical attraction, nucleation growth of crystallites in nanometric length variation and change in particle size.

EDX studies: The EDX spectrum confirms the presence of oxygen (O) and molybdenum (Mo) [16]. The atomic percentage of oxygen decreases with the increase in concentration whereas the atomic percentage of molybdenum increases with the increase in concentration (Table-2). The elemental analysis confirms the absence of impurities in the prepared samples as shown in Fig. 6.

FTIR studies: The molecular vibrations of the groups present in the sample is analyzed using FT-IR spectra. Fig. 7 shows the FT-IR spectrum of prepared MoO_3 thin films. The prominent peaks are observed at 563, 864, 995 and 1126 cm^{-1} [17]. The vibrating mode at 563 cm^{-1} is due to the stretching mode of triply coordinated oxygen ν(O-Mo_3). The peaks around 864 cm^{-1} is due to the stretching mode of doubly coordinated oxygen (νO-Mo_2) and the peak at 995 cm^{-1} is attributed to the stretching mode of terminal oxygen ν(O=Mo). The peak at 1126 cm^{-1} is due to the bending mode of Mo-OH bonds δ(Mo-OH) [18,19]. Thus, the formation of MoO_3 thin films is confirmed using FT-IR spectra.

Raman studies: Fig. 8 shows the Raman spectra of MoO_3 samples. Raman spectroscopy gives the structural information

TABLE-1
ESTIMATED STRUCTURAL PARAMETERS OF MoO_3 THIN FILMS

MoO_3 (mole fraction)	2θ (°)	hkl	d-spacing (nm)	FWHM (°)	Grain size (D) (nm)	Dislocation density (10^{14} lines/m^2)	Micro-strain (ε) 10^4 lin^{-2} m^{-4}	Lattice constants (Å)		
								a	b	c
1%	23.47	110	3.7858	0.3559	23.81	0.001763	0.152042	3.95	13.82	3.68
	25.79	120	3.4505	0.3097	27.48	0.001323	0.131721			
	27.43	021	3.2485	0.2725	31.34	0.001017	0.133092			
2%	23.43	110	3.7962	0.3483	24.32	0.001689	0.148813	3.96	13.86	3.68
	25.75	120	3.4589	0.3070	27.72	0.001301	0.130590			
	27.31	021	3.2547	0.2693	31.71	0.000994	0.114165			
3%	23.23	110	3.8174	0.3489	24.28	0.001696	0.149104	3.99	13.74	3.68
	25.67	120	3.4764	0.3088	27.55	0.001317	0.131390			
	27.21	021	3.2702	0.2807	30.04	0.001080	0.119032			
4%	23.47	110	3.7937	0.4739	17.88	0.003127	0.202470	3.96	13.81	3.68
	25.78	120	3.4505	0.4780	17.80	0.003153	0.203303			
	27.33	021	3.2544	0.5709	14.95	0.004468	0.242023			

TABLE-2
ELEMENTAL COMPOSITION OF MoO_3 THIN FILMS

Element	L1		L2		L3		L4	
	Weight (%)	Atomic (%)	Weight (%)	Atomic (%)	Weight (%)	Atomic (%)	Weight (%)	Atomic (%)
OK	46.78	85.33	47.57	84.47	45.67	82.60	38.49	78.96
MoL	53.22	14.67	52.43	15.52	54.33	17.40	61.51	21.04

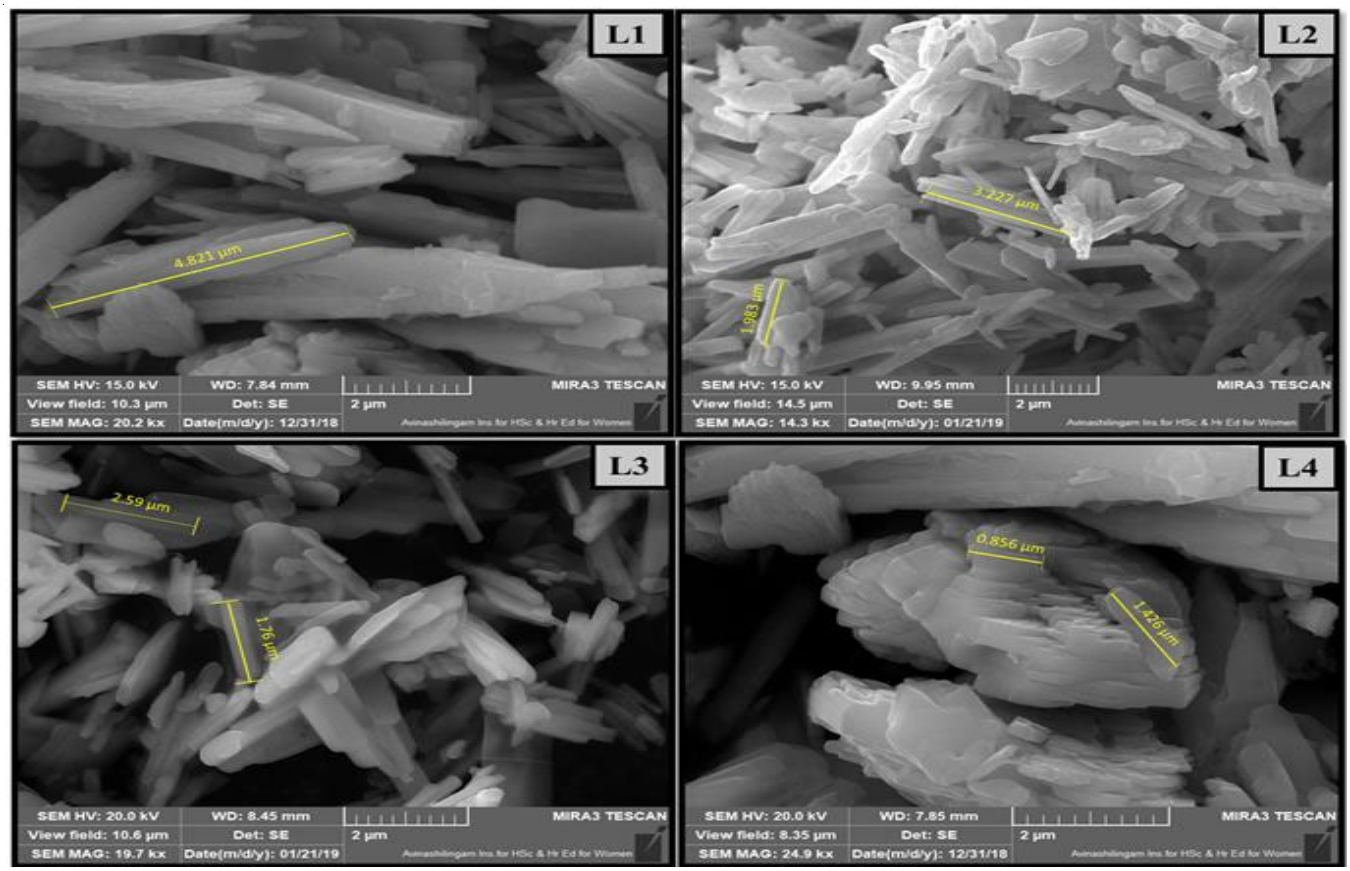

Fig. 5. FE-SEM images of MoO_3 thin films

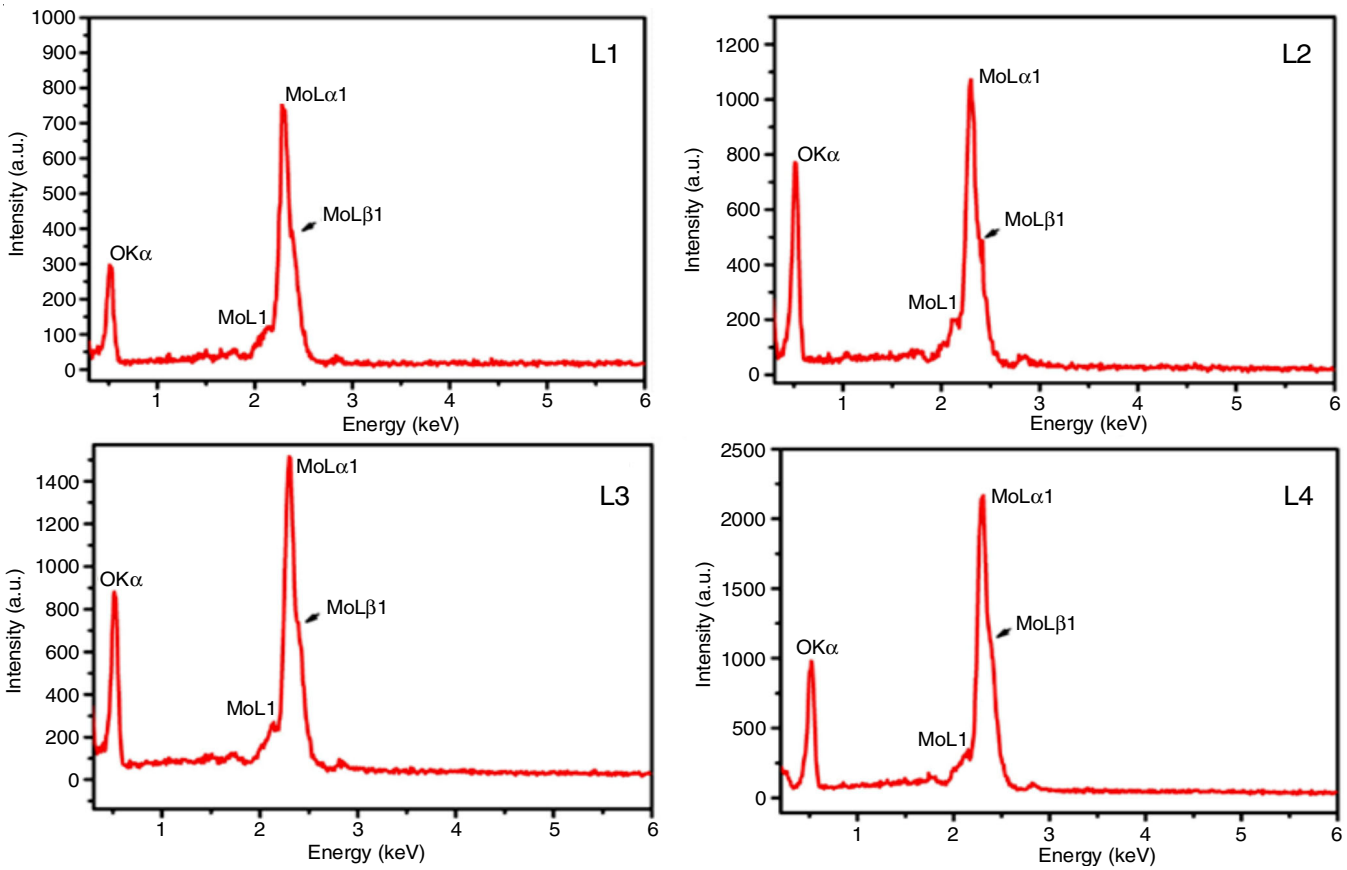

Fig. 6. EDX spectrum of MoO_3 thin films

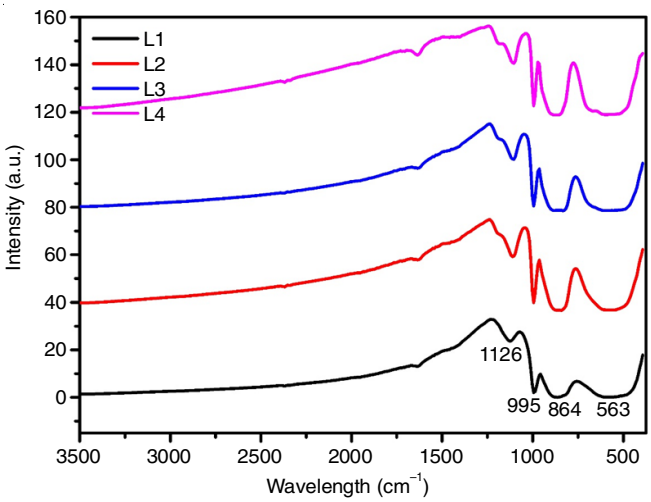

Fig. 7. FT-IR spectra of MoO_3 thin films

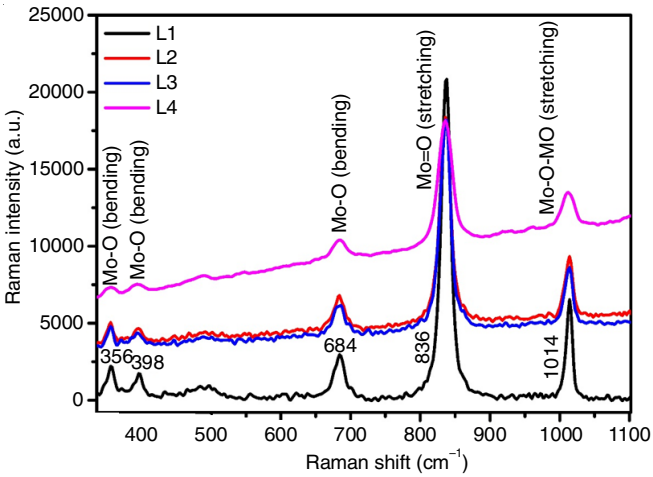

Fig. 8. Raman spectra of MoO_3 thin films

mainly on the vibrational properties of the synthesized samples. The obtained Raman peaks located at 356, 398, 684, 836 and 1014 cm^{-1} correspond to orthorhombic α-MoO_3 phase belonging to the space group *Pbnm*. In this space group, MoO_3 unit cell contains 4 molybdenum atoms and 12 oxygen atoms [20]. This property is expressed in terms of displacement of atoms by 48 eigen modes in the centre of the Brillouin zone [21]. In general, the irreducible representation can be given by a linear combination of active modes A_g, B_{1g}, B_{2g}, B_{3g}, A_u, B_{1u}, B_{2u} and B_{3u} using the formula:

$$\Gamma = 8A_g + 8B_{1g} + 4B_{2g} + 4B_{3g} + 4A_u + 3B_{1u} + 7B_{2u} + 7B_{3u}$$

The intensity of the positive peak reveals a good crystallization of prepared films. The vibrational analysis of Raman spectra reveals that the band in 900-500 and 500-200 cm^{-1} regions are mainly due to Mo-O stretching and bending modes respectively. The nature of α-MoO_3 is confirmed by the peaks at 1014, 836 and 684 cm^{-1}. The Raman peaks at 1014 cm^{-1} belongs to Mo-O-MO stretching vibrations of terminal unshared oxygen. The sharp intense peak at 836 cm^{-1} arises from the O-Mo_2 doubly connected bridging bond of corner shared oxygen [22,23]. The peak at 684 cm^{-1} of triply coordinated bridge-oxygen (O-Mo_3) is from edge shared oxygen. Raman active modes having low intensity at 398, 356 cm^{-1} assigned to the Mo-O bending mode can be attributed to O-Mo-O scissoring and O=Mo=O wagging modes. These results support the formation of α-MoO_3 thin films using spray pyrolysis method.

Photoluminescence studies: The photoluminescence (PL) spectral plot is shown in Fig. 9. The optical properties of MoO_3 were investigated from the photoluminescence studies. The main emission peak of α-MoO_3 was found to be centered at 305, 308, 310, 314 nm for 1% and 2%, 3% and 4% molar concentration of MoO_3, respectively. It is observed that the PL curve seems to be similar in all conditions except the band edge absorption rates. From the curve, it is obvious that the peak relative intensity possess higher values with increase in molar concentration.

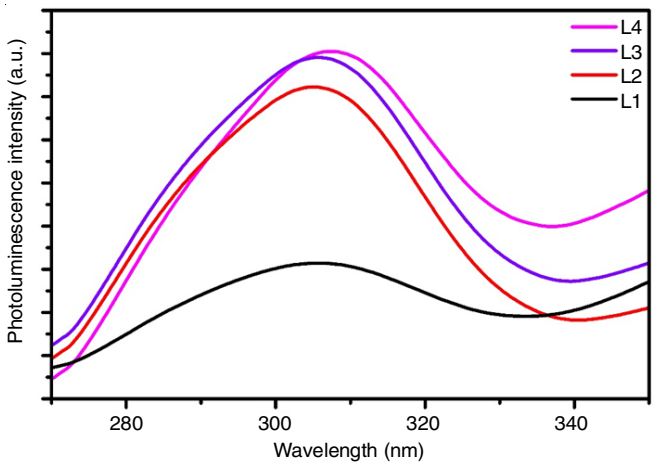

Fig. 9. Photoluminescence spectra of MoO_3 thin films

It is reported that PL intensity of α-MoO_3 rods is relatively weaker, the lower recombination rate of photogenerated electron-hole pairs [24]. It is also clearly evident that the location of PL band and PL intensity changes with the nature of the substrate used [25,26].

I-V characteristics of n-MoO_3/p-Si: The 4 wt.% Mo concentration MoO_3 prepared sample at 450 ºC was used to fabricate p-n heterojunction diode on p-type Si wafer using JNPS techniques. Fig. 10a gives the structural arrangement of pure n-MoO_3/p-Si structure diode. The I-V current voltage characteristics curve is plotted by taking the measurement of forward and reverse current values for pure n-MoO_3/p-Si structure SBDS were done by applying voltage from -2 V

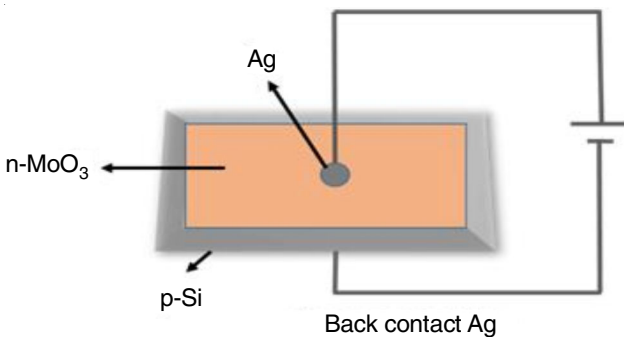

Fig. 10(a). The device structure of MoO_3

to +2 B (in steps of 0.4 V) and from Fig. 10b, it is clearly understood that the device exhibits asymmetric and nonlinear behaviour.

Fig. 10c depicts the semi-logarithmic float of current density (ln J) *versus* voltage (V for pure MoO_3/p-Si diode) the parameters where analyzed, under illumination source of a halogen lamp and in darkness condition. It was observed that diode exhibits the rectification behaviour, under dark condition.

The rectification ratio (RR) can be estimated by finding the ratio of forward current density (J_F) to the reverse current density (J_R), at a certain applied voltage (V), which can be expressed as $RR = (J_F/J_R)^V$. The thermionic emission current voltage dependence of the junction of the given voltage can also be considered which can be found out by using eqn. 4:

$$I = I_s\left[\exp\left(\frac{qV}{nKT}\right)-1\right]\left(V \geq 3K_b\frac{T}{q}\right) \quad (4)$$

where V is the applied bias voltage (expressed in volts), I is the measured current, I_s is the saturation current and absolute value of electronic charge (in C) is q, K_b and T are Boltzmann's constant and absolute temperature respectively, n is the ideality factor (n = 1, for ideal condition and n > 1, if transport mechanism was not governed exclusively by a thermionic emission process). The saturation current I_s can be calculated by using eqn. 5:

$$I_s = AA^* T^2 \exp\left(-\frac{q\Phi_B}{KT}\right) \quad (5)$$

where A^* is the theoretical Richardson constant, A is the diode area Φ_B is the zero bias barrier height. The ideality factor n can be calculated from the slope straight line region during the forward bias I-V plot that can be expressed by eqn. 6:

$$n = \frac{q}{KT}\frac{dV}{d(\ln I)} \quad (6)$$

where I_0 can be extrapolation of forward bias in I-V curve at V = 0, the Φ_B can be calculated by using eqn. 7:

$$\Phi_B = \frac{KT}{q}\ln\left(\frac{AA^* T^2}{I_o}\right) \quad (7)$$

where I_o, q, v, n, KB, T and A^* is the reverse leakage current density, electron charge, applied voltage, ideality factory, Boltzman constant, temperature in K and effective Richardson constant for p type silicon wafer, respectively.

The ideality factor can also be calculated from the slope of the intercept of the semi lograthmic forward biased J-V plot, the ideality factor (n and barrier height φB) values for MoO_3 were calculated and the values are given in Table-3 for the dark and light illumination condition [27]. The value of the ideality factor and barrier height found to increase in values for the same condition as shown in Table-1. It is found that the ideality factor and the barrier height increase with increase in temperature for pure MoO_3/p-Si diode structure.

TABLE-3
ELECTRICAL PARAMETERS OF THE MoO_3 DIODE

Sample	Ideality factor (n)	Barrier height (Φ_B)	Saturated current (I_o)
MoO_3	1.4855	0.40972	5.41×10^{-5}

The n and Φ_B values were found to be 1.485 and 0.409 respectively, in dark and under illumination conditions for the diodes.

Conclusion

In conclusion, successful deposition of molybdenum trioxide (MoO_3) thin films with various Mo concentrations 1, 2, 3 and 4 wt.% on to the silica substrate calcined at 450 °C by a facile, rapid, cost effective and a custom-made jet nebulizer spray pyrolysis (JNSP) technique is reported. The concentration impact on the structural, morphological and compositional parameters of the fabricated films were examined. The structural analysis by XRD confirms the presence of orthorhombic phase of MoO_3 in the prepared sample with preferential orientation

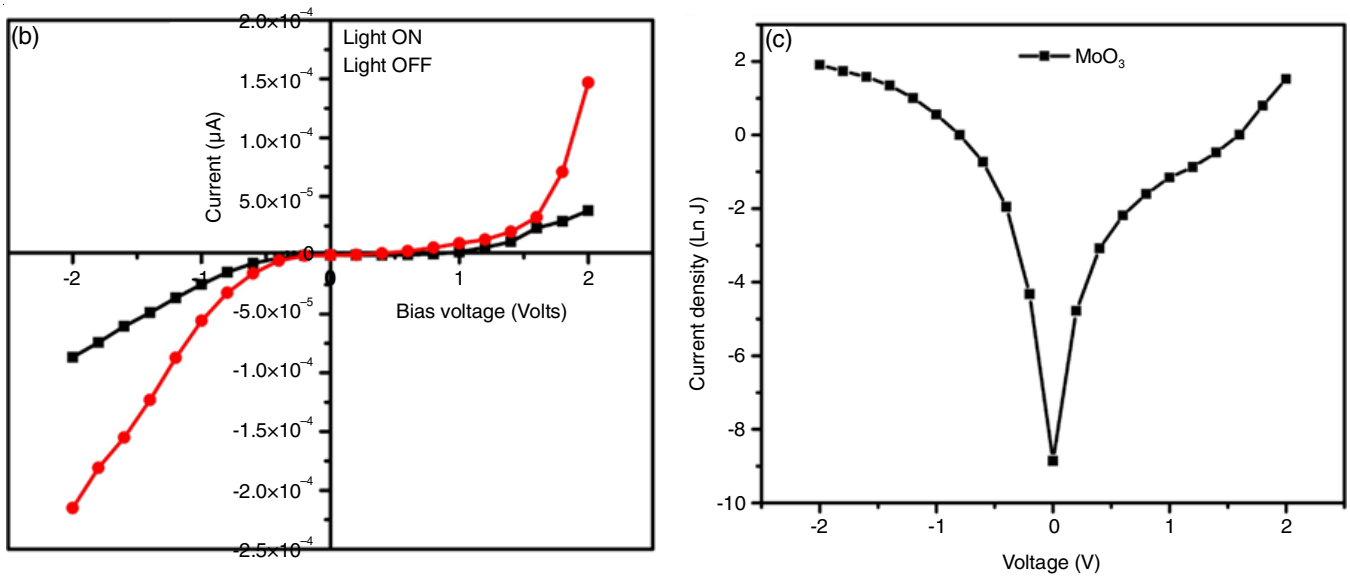

Fig. 10. I-V curve of (b) n-MoO_3/p-Si, I-V curve of (c) current density (J)-voltage (V) plots of n-MoO_3/p-Si diodes

at (110), (120) and (021) planes. Crystallite sizes were decreasing from 32-15 nm whereas the microstrains increased between ~ 0.11 and 0.24 lin^{-2} m^{-4} while increasing the Mo concentrations. Morphologies of the fabricated samples resembling nano-structured rods were observed in the FESEM images. The wide spread distribution of a crack free homogeneous surface reveals the good adhesion of the deposited films on to the silica substrates. The various vibration levels residing in the samples were detected through FTIR (vibration levels in the infrared regions) and Raman studies (molecular vibration levels). As a whole this work revealed that different Mo concentrations plays a vital role in determining the structural, morphological and compositional parameters of the coated films. The ideality factor (1.4855) and barrier height (0.40972 eV) was obtained for 4 wt.% of Mo concentration of the prepared sample.

CONFLICT OF INTEREST

The authors declare that there is no conflict of interests regarding the publication of this article.

REFERENCES

1. A.I. Hassan and S.I. Maki, *Energy Procedia*, **119**, 961 (2017); https://doi.org/10.1016/j.egypro.2017.07.129
2. W. Li, J. Shi, K.H.L. Zhang and J.L. MacManus-Driscoll, *Mater. Horiz.*, **7**, 2832 (2020); https://doi.org/10.1039/D0MH00899K
3. X.W. Lou and H.C. Zeng, *Chem. Mater.*, **14**, 4781 (2002); https://doi.org/10.1021/cm0206237
4. I.A. de Castro, R.S. Datta, J.Z. Ou, A. Castellanos-Gomez, S. Sriram, T. Daeneke and K. Kalantar-zadeh, *Adv. Mater.*, **29**, 1701619 (2017); https://doi.org/10.1002/adma.201701619
5. T.V. Sviridova, L.Y. Sadovskaóa, E.M. Shchukina, A.S. Logvinovich, D.G. Shchukin and D.V. Sviridov, *J. Photochem. Photobiol. Chem.*, **327**, 44 (2016); https://doi.org/10.1016/j.jphotochem.2016.04.018
6. T. Nagyné-Kovács, L. Studnicka, I.E. Lukács, K. László, P. Pasierb, I.M. Szilágyi and G. Pokol, *Nanomaterials*, **10**, 891 (2020); https://doi.org/10.3390/nano10050891
7. T. Anh Tran, K. Krishnamoorthy, Y.W. Song, S.K. Cho and S.J. Kim, *ACS Appl. Mater. Interfaces*, **6**, 2980 (2014); https://doi.org/10.1021/am405586d
8. T. Waters, R.A. O'Hair and A.G. Wedd, *J. Am. Chem. Soc.*, **125**, 3384 (2003); https://doi.org/10.1021/ja028839x
9. L. Zhang, G. Wu, F. Gu and H. Zeng, *Sci. Rep.*, **5**, 17388 (2015); https://doi.org/10.1038/srep17388
10. W. Seiler, E. Millon, J. Perrière, R. Benzerga and C. Boulmer-Leborgne, *J. Cryst. Growth*, **311**, 3352 (2009); https://doi.org/10.1016/j.jcrysgro.2009.03.047
11. L. Boudaoud, N. Benramdane, A. Bouzidi, A. Nekerala and R. Desfeux, *Optik*, **127**, 852 (2016); https://doi.org/10.1016/j.ijleo.2015.10.105
12. C.R. Dhas, D. Alexander, A.J. Christy, K. Jeyadheepa, A.M.E. Raj and C.S. Raja, *Asian J. Appl. Sci.*, **7**, 671 (2014); https://doi.org/10.3923/ajaps.2014.671.684
13. K. Ravichandran, A. Manivasaham, K. Subha, A. Chandrabose and R. Mariappan, *Surf. Interfaces*, **1-3**, 13 (2016); https://doi.org/10.1016/j.surfin.2016.06.004
14. N.G. Prakash, M. Dhananjaya, A.L. Narayana, H. Maseed, V.V.S.S. Srikanth and O.M. Hussain, *Appl. Phys., A Mater. Sci. Process.*, **125**, 488 (2019); https://doi.org/10.1007/s00339-019-2779-2
15. A. Klinbumrung, T. Thongtem and S. Thongtem, *J. Nanomater.*, **2012**, 930763 (2012); https://doi.org/10.1155/2012/930763
16. G. Pradeep, V. Ponnuswamy, B. Gowtham, J. Chandrasekaran and R. Suresh, *Optik*, **175**, 217 (2018); https://doi.org/10.1016/j.ijleo.2018.09.020
17. T. Chiang and H. Yeh, *Materials*, **6**, 4609 (2013); https://doi.org/10.3390/ma6104609
18. N. Rajiv Chandar, S. Agilan, R. Thangarasu, N. Muthukumarasamy and R. Ganesh, *J. Mater. Sci. Mater. Electron.*, **31**, 7378 (2020); https://doi.org/10.1007/s10854-019-02820-w
19. S. Patnaik, G. Swain and K.M. Parida, *Nanoscale*, **10**, 5950 (2018); https://doi.org/10.1039/C7NR09049H
20. J.V.B. Moura, J.V. Silveira, J.G. da Silva Filho, A.G. Souza Filho, C. Luz Lima and P.T.C. Freire, *Vib. Spectrosc.*, **98**, 98 (2018); https://doi.org/10.1016/j.vibspec.2018.07.008
21. R. Sharma, R. Jha, A. Sarkar, A.K. Sharma, D. Sharma, M. Bhushan and R. Bhardwaj, *Ceram. Int.*, **46**, 23084 (2020); https://doi.org/10.1016/j.ceramint.2020.06.085
22. A.E.X. Gavim, M.R.P. da Cunha, E.R. Spada, T.N. Machado, F.S. Hadano, A. Ginane Bezerra Jr., W. Herwig Schreiner, P.C. Rodrigues, A. Rashid bin Mohd Yusoff, A.G. Macedo, R.M. Faria and W.J. da Silva, *Energy Mater. Sol. Cells.*, **200**, 109986 (2019); https://doi.org/10.1016/j.solmat.2019.109986
23. A. Boukhachem, O. Kamoun, C. Mrabet, C. Mannai, N. Zouaghi, A. Yumak, K. Boubaker and M. Amlouk, *Mater. Res. Bull.*, **72**, 252 (2015); https://doi.org/10.1016/j.materresbull.2015.08.011
24. H. Hu, C. Deng, J. Xu, K. Zhang and M. Sun, *J. Exp. Nanosci.*, **10**, 1336 (2015); https://doi.org/10.1080/17458080.2015.1012654
25. N. Illyaskutty, S. Sreedhar, G. Sanal Kumar, H. Kohler, M. Schwotzer, C. Natzeck and V.P.M. Pillai, *Nanoscale*, **6**, 13882 (2014); https://doi.org/10.1039/C4NR04529G
26. N. Benameur, M.A. Chakhoum, A. Boukhachem, M.A. Dahamni, M. Ghamnia, N. Hacini, J.P. Pireaux, L. Houssiau and A. Ziouche, *J. Electron. Spectrosc. Rel. Phenom.*, **234**, 71 (2019); https://doi.org/10.1016/j.elspec.2019.05.015
27. P. Vivek, J. Chandrasekaran, R. Marnadu, S. Maruthamuthu, V. Balasubramani and P. Balraju, *Optik*, **199**, 163351 (2019); https://doi.org/10.1016/j.ijleo.2019.163351